

**Study report on
the LCGT Suspension Point Interferometer**

LCGT SPI Special Working Group
September 7, 2009 (Revised November 8, 2009)

Contents

1	Executive summary	3
1.1	Recommendations	3
1.2	Summary of the reasoning behind the recommendations	3
2	Expected performance of the LCGT SPI	4
2.1	Suspension Model	4
2.2	Observation band seismic noise	4
2.3	RMS motion	4
2.3.1	Displacement RMS	4
2.3.2	Hierarchical control	7
2.3.3	Speed RMS	8
3	Heat link vibration isolation	8
3.1	Heat-link design	8
3.2	Estimated vibration introduced from the heat-links	10
3.3	Cryogenic active vibration isolation	11
3.4	Conclusion for heat-link vibration isolation	12
4	Lock acquisition	12
4.1	LCGT lock acquisition procedure	12
4.2	Obstacles for arm cavity lock	13
4.2.1	Impulse limit velocity for mass lock acquisition	13
4.2.2	Ringling velocity	14
4.2.3	Radiation pressure	14
4.2.4	Arm lock simulation	15
4.3	Advanced lock acquisition techniques	16
4.3.1	Offset locking	16
4.3.2	Green laser pre-lock	16
4.4	Conclusion for lock acquisition	17
5	Vacuum tubes	18
A	Design of the LCGT Suspension Point Interferometer	19
A.1	Working Principle	19
A.1.1	Rigid Bar Picture	20
A.2	Design of the LCGT SPI	20
A.2.1	Interferometer Configuration	21
A.2.2	Location of SPI in the Suspension Chain	22
A.2.3	Suspension Design	23
A.2.4	Noise Requirement	25
A.2.5	Input Optics	26
A.2.6	Comments on technical feasibility	27
B	Members of the working group	27
C	Acronyms	29

1 Executive summary

The LCGT SPI special working group is charged with the investigations on the necessity and feasibility of the suspension point interferometer for LCGT. The biggest question to be answered is whether we need to install an SPI to LCGT or not. For this purpose, we examined the necessity of the SPI mainly from two aspects: (1) the reduction of the vibration introduced from heat-link wires and (2) the reduction of RMS mirror motion for robust lock acquisition. We also investigated alternative techniques which can replace or supplement the SPI.

This document is a result of the discussions in the working group. In this section, we present our recommendations and a brief explanation of the reasoning behind them. Model calculations are presented in section 2 to show the expected performance of the LCGT SPI. In section 3, we will examine the necessity of the SPI for heat-link vibration isolation. The lock acquisition scheme for LCGT is reviewed in section 4 and the importance of SPI as a lock acquisition aid is assessed. Finally the current design of the LCGT SPI is discussed in section A.

1.1 Recommendations

The LCGT SPI special working group proposes the following actions be taken regarding the LCGT SPI.

Recommendations

- We shall not install an SPI for LCGT
- We shall continue to put R&D efforts on the alternative techniques, such as cryogenic active vibration isolation stage (section 3.3), hierarchical control (section 2.3.2), offset lock (section 4.3.1) and green laser pre-lock (section 4.3.2).
- In order to keep the possibility of retrofitting an SPI in the future, we shall keep the vacuum tube size large enough (1 m). The beam height of the main laser in the vacuum tube shall be offset from the center to accommodate the SPI beam in the future.

1.2 Summary of the reasoning behind the recommendations

The above recommendations were drawn from the following reasons.

- Simulations show that the target sensitivity of LCGT is not compromised by the heat-link vibration even without an SPI (figure 3).
- The seismic noise is limited by the vertical vibration coupling from the heat-links above 6 Hz (i.e. in the observation band). Since vertical vibrations cannot be suppressed by an SPI, an improvement of the seismic noise safety factor cannot be expected from SPI.
- LCGT's requirement for the RMS displacement noise ($0.1 \mu\text{m}$ above 0.1 Hz) is satisfied without an SPI in the normal seismic period (figure 4). When the micro seismic motion is high, the RMS is estimated to be $0.2 \mu\text{m}$, which is only a factor of two above the requirement (figure 5). We do not think it is worth spending a lot of resources on SPI to reduce this by a factor of 2. Moreover, almost the same effect as the RMS reduction by the SPI can be achieved by a carefully designed hierarchical control (section 2.3.2).
- To avoid a large kick by the radiation pressure, we will use the offset lock technique for the lock acquisition regardless of the seismic noise (section 4.2.3). Since the offset lock has a larger linear range than the PDH signal, the lock acquisition can be robust even without an SPI.
- In order to give more safety margins to both the observation band seismic noise and the RMS motion, we should pursue alternative techniques for the suppression of the heat-link vibration and robust lock acquisition. The alternative techniques proposed in this report

are not intrusive to the core part of the interferometer and easily retrofitted when the technology is ready. In contrast, the SPI requires a major modification to the penultimate mass design. If it fails, there is a risk of degrading the interferometer sensitivity. Considering the current maturity of the LCGT SPI design study, we estimate that resources necessary to successfully implement a practical SPI to LCGT is much more than the cost required to develop these alternative techniques.

- Even though SPI is not necessary for the current LCGT, next generation upgrades to the LCGT may require an SPI. We may also want to use a larger beam size in the future. Since it is very costly to replace the vacuum envelope once it is built, we have to have a margin for future upgrades. Therefore, we propose to keep the beam tube size the same as the original design (1 m diameter).

More detailed discussion and calculations to support the above reasoning will be presented in the following sections.

2 Expected performance of the LCGT SPI

2.1 Suspension Model

In order to estimate the performance of the LCGT SPI, we developed a one dimensional model of the LCGT suspension systems with an SPI. A conceptual diagram of the LCGT suspension system is shown in figure 1. The overall height of the suspension is about 4 m. This model includes heat-links connecting the 4 K cryo-shield and the suspension platform. Details of the heat-link design is explained in section 3.

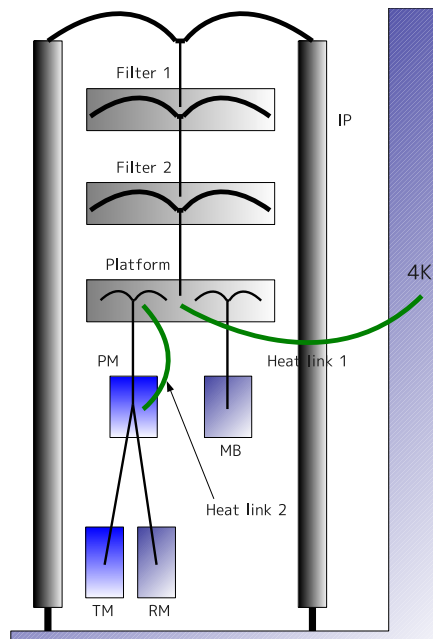


Figure 1: Conceptual diagram of the LCGT suspension system. IP: Inverted Pendulum, PM: Penultimate Mass, MB: Magnet Box, TM: Test Mass, RM: Recoil Mass.

The SPI is formed at the PM (penultimate mass) stage. The feedback filter for the SPI servo is made to set the unity gain frequency around 50 Hz. This filter has a low frequency gain boost. The overall open loop transfer function of the SPI servo is shown in figure 2.

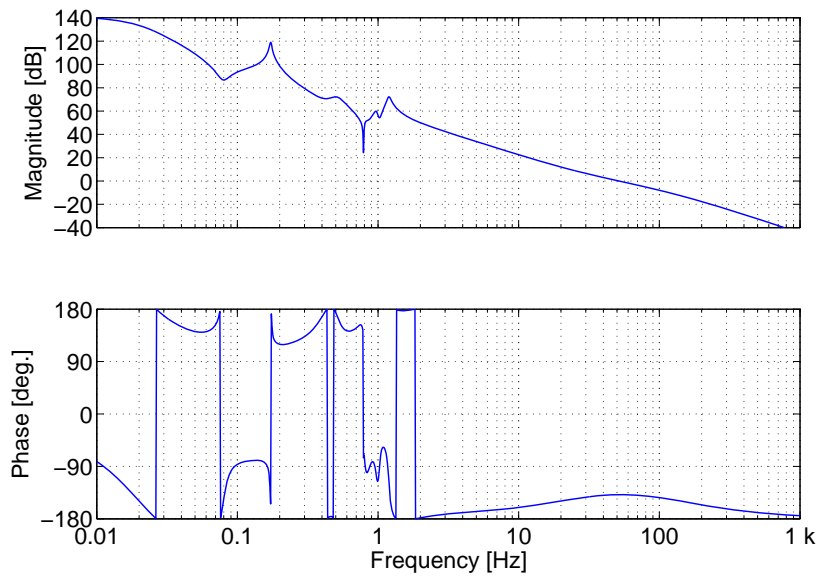


Figure 2: SPI servo's open loop transfer function

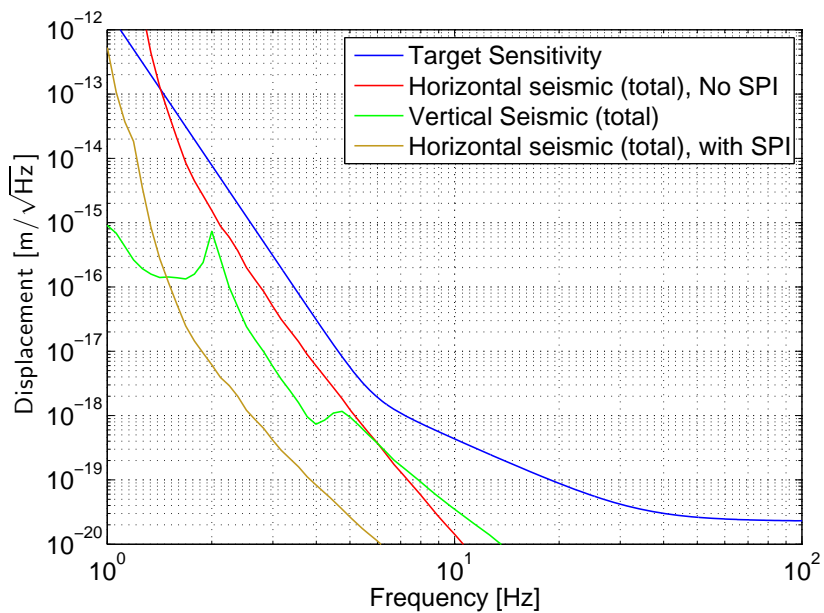


Figure 3: Seismic noise and the LCGT target sensitivity.

2.2 Observation band seismic noise

The seismic noise contribution to the LCGT noise is calculated using the above mentioned model. Figure 3 shows the estimated seismic noise with and without the SPI along with the target sensitivity of LCGT. The vertical seismic noise was calculated by an independent one dimensional vertical suspension model and assuming 1% vertical-to-horizontal coupling.

The seismic noise does not limit the sensitivity of the interferometer above 2 Hz even without the SPI. The safety margin for the seismic noise without SPI is more than a factor of 6 above 5 Hz. The horizontal seismic noise can be suppressed by the SPI by more than 20 dB. However, the vertical noise coupling becomes dominant above 6 Hz. Therefore, the ability of the SPI to reduce the seismic noise in the observation band is very limited.

2.3 RMS motion

2.3.1 Displacement RMS

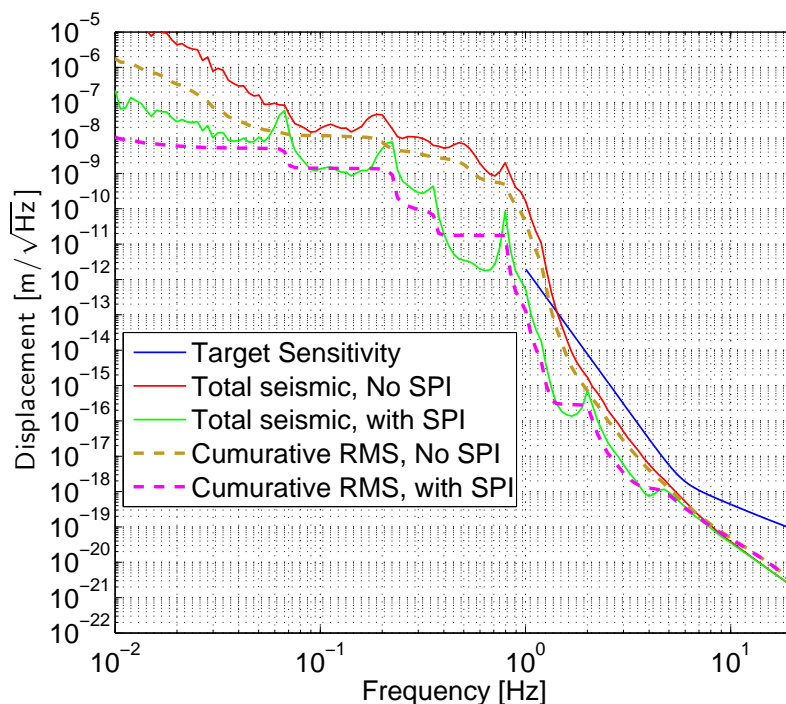


Figure 4: RMS displacement noise when the seismic noise is normal. Total Seismic means the overall motion of the mirrors caused by all kinds of seismic vibrations.

Displacement RMSs of the test masses are calculated by integrating the displacement noise spectra (figure 4). LCGT's requirement for the displacement RMS is less than 100 nm integrated above 0.1 Hz. It is an RMS of the open-loop mirror motion (the motion of the mirror which will occur if there is no feedback from the interferometer signal). The estimated RMS is 10 nm for the no-SPI case and 1 nm with the SPI. Therefore, the requirement is satisfied even without the SPI.

When there is a storm outside, the micro seismic motion in the Kamioka mine becomes high. Roughly speaking, such a condition happens once a week during the winter (Dec. - Mar.) and once a month in the other seasons. Figure 5 shows the seismic noise spectra calculated with a typical ground motion spectrum of high micro seismic times. In this case, the RMS displacement is 200 nm without the SPI and 20 nm with the SPI. The no-SPI case slightly exceeds the requirement.

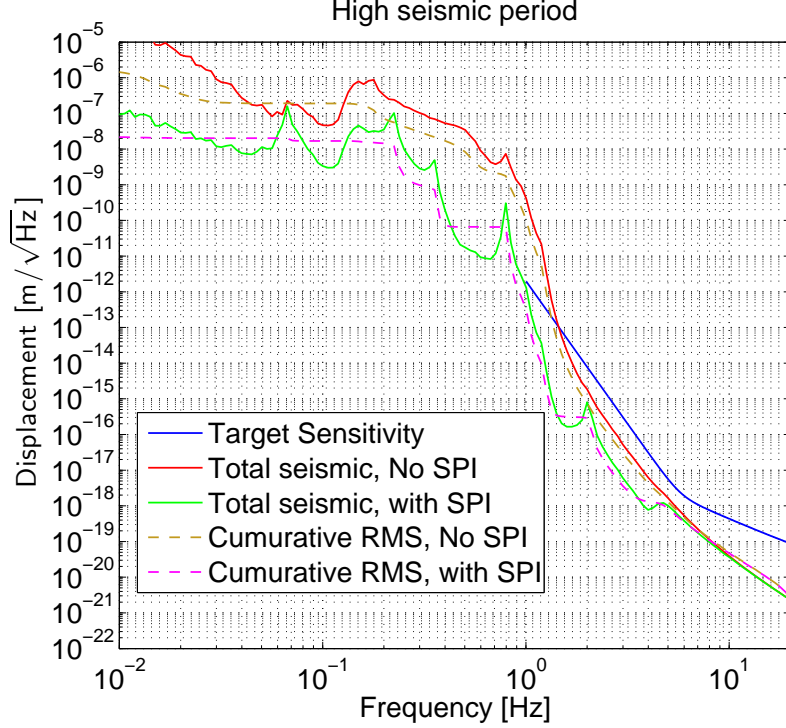


Figure 5: RMS displacement noise when the micro seismic motion is high. Total Seismic means the overall motion of the mirrors caused by all kinds of seismic vibrations.

An important thing to notice is that the seismic noise is still below the target sensitivity in the high seismic period. This is because the heightened micro-seismic motion only affects frequencies below 1 Hz. Up conversions of large low frequency noise through non-linearity of the detector response could still be a problem. However, this problem can be mitigated by the hierarchical control discussed below.

2.3.2 Hierarchical control

A large RMS displacement noise can make the interferometer unstable. Resultant frequent lock losses will decrease the duty cycle of the detector. We also have to increase the control bandwidths of the auxiliary degrees of freedom, such as the Michelson part, to keep the interferometer at the operational point against large low frequency excitations. This may increase the control noise couplings. Also up conversion of the low frequency noises to the observation band through non-linearities in the detector can be serious.

The above problems all arise from insufficiently suppressed residual motion of the test masses. One way to solve this problem is to reduce the noise itself, which is what an SPI is supposed to do. Another solution is to increase the servo gain and strongly suppress the residual motion.

In general, we cannot make the test mass actuators too strong because the actuator noise then contaminates the sensitivity. However, if we feedback the error signal to the upper stages of the suspension system, the actuator noises are naturally filtered out at high frequencies, thus not contaminating the observation band sensitivity. A hybrid actuator formed by strong upper stage actuators for low frequencies and weak test mass actuators for high frequencies will allow us to strongly suppress the low frequency vibrations. This scheme is called hierarchical control.

Actually, there is an equivalence principle between SPI and hierarchical control. The SPI senses the same degree of freedom as the main interferometer (beam direction) and feed the signal back to the penultimate stage actuators. Since there is a linear relationship between the motion of the penultimate masses and the test masses, the main interferometer can obtain the same information as the SPI unless the seismic motion is attenuated below other noises by the

final stage pendulum, in which case we don't care the seismic noise anyway. Feeding back the error signal from the main interferometer to the penultimate stage is therefore equivalent to an SPI's action in principle.

However, there are two important differences. One is that the hierarchical control cannot reduce the seismic "noise" appearing at the gravitational wave channel. It only reduces the residual motion of the mirrors. The other difference is that the SPI can suppress the noise of the SPI actuators by the servo, whereas the hierarchical control does not have this active suppression. It has only passive attenuation by the suspension transfer function.

Even with these differences, still the hierarchical control can provide most of the benefits of SPI regarding the RMS reduction.

One thing to note is that the hierarchical control only works when the interferometer is locked. Therefore, it cannot be used to reduce the RMS speed of the test masses to help lock acquisition.

It is also worth mentioning that hierarchical control schemes have been successfully implemented by VIRGO and GEO [refs]. Advanced LIGO will also employ this actuation topology. We should make use of the experiences accumulated by those projects when designing the LCGT hierarchical control.

2.3.3 Speed RMS

The mirror speed spectra are shown in figure 6 for a normal seismic period and figure 7 for a high micro seismic period.

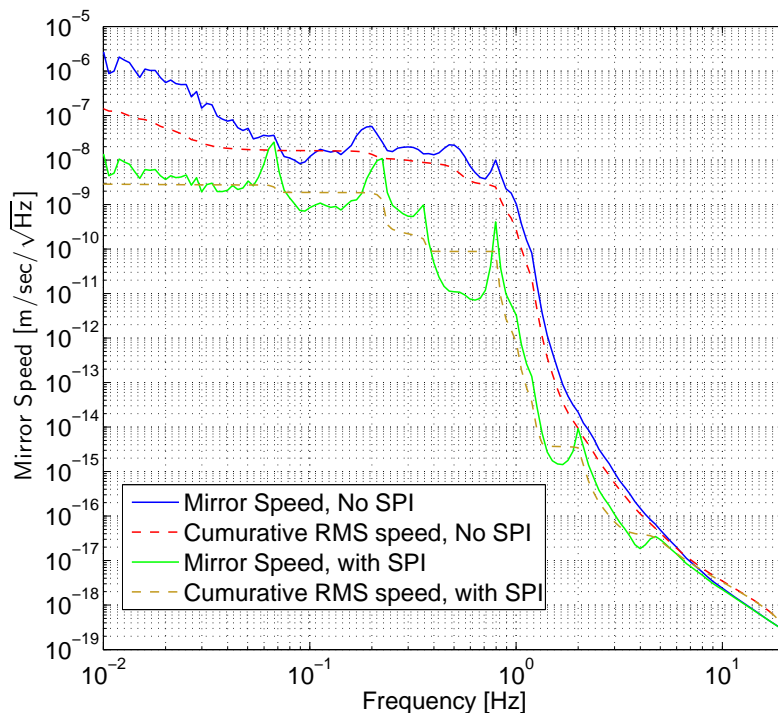


Figure 6: Mirror RMS speed

The RMS mirror speed for the normal seismic period is 20 nm/sec without the SPI and 2 nm/sec with the SPI (integrated above 0.1 Hz). It becomes 200 nm/sec (no SPI) and 20 nm/sec (with SPI) when the micro seismic activity is high.

The mirror speed mainly affects the robustness of the lock acquisition. Since we do not have to worry about the sensitivity of the interferometer at this stage, we may be able to reduce the

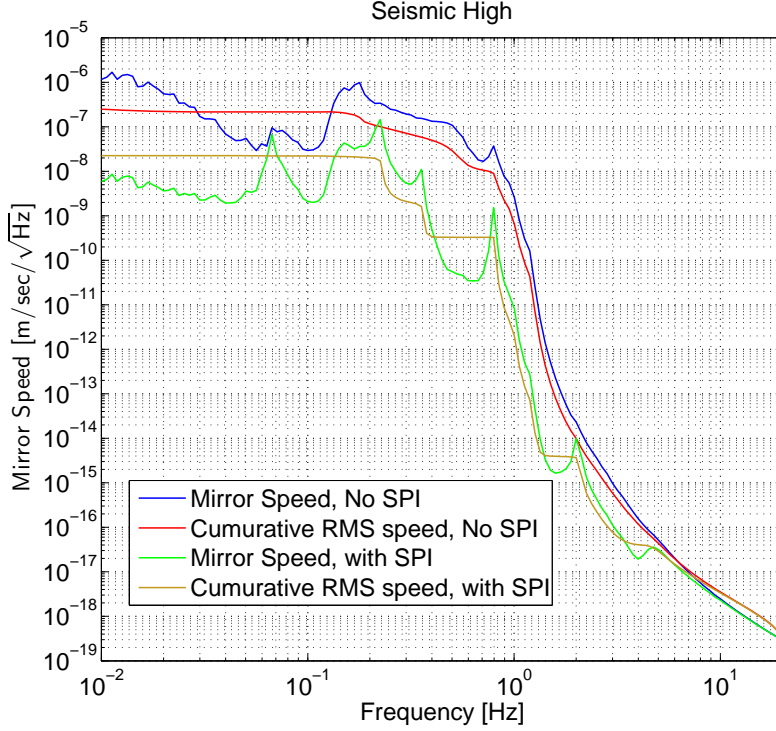


Figure 7: Mirror RMS speed when the micro seismic motion is high

RMS speed by applying aggressive damping to the suspension system. Other lock acquisition tricks are discussed in section 4.

3 Heat link vibration isolation

In this section, we discuss the necessity of SPI for heat-link vibration isolation.

3.1 Heat-link design

The heat-links used to subtract heat from the mirrors are 99.9999% pure aluminum wires. 7 heat-links with 1 mm diameter connect the suspension platform and the cryo-shield. These are U shaped with the radius of curvature 25 cm. The platform and the penultimate mass are connected by 5 heat-links with the diameter 3 mm. These are U shaped with 20 cm ROC.

The spring constants of a U shaped wire can be calculated by the following formulae.

$$k_x = \frac{Ed^4}{32R^3} \quad (1)$$

$$k_y = \frac{Gd^4}{32R^3} \quad (2)$$

$$k_z = \frac{Ed^4}{96R^3} \quad (3)$$

E is the Young's modulus, G is the shear modulus, d is the diameter of the wire and R is the bending radius of curvature. Since $E > G$ for aluminum, k_x has the largest value among the three.

Combined with the 120 kg mass of the suspension platform, the resonant frequency of a mass-spring system formed by the platform and the heat-links is about 14 mHz for x -direction and 8 mHz for z -direction. These values are used in the suspension model explained in section 2.1.

As one can see in the above formulae, the stiffness of the heat-links is proportional to the fourth power of the wire diameter. On the other hand, the thermal conductivity of the wire is proportional to the cross section of the wires ($\propto d^2$). Therefore, we can increase the number of heat-links keeping the total cross section constant to reduce the stiffness of the heat links if necessary.

The above mentioned model of the heatlink takes into account only the stiffness arising from static deformations of a heatlink, which is a good approximation for low frequency behavior of the heatlink. However, it does not include the inertia of the heatlink mass nor the internal vibration modes. For more accurate estimates of the vibration isolation performance of heatlinks, we should perform detailed finite element analyses.

3.2 Estimated vibration introduced from the heat-links

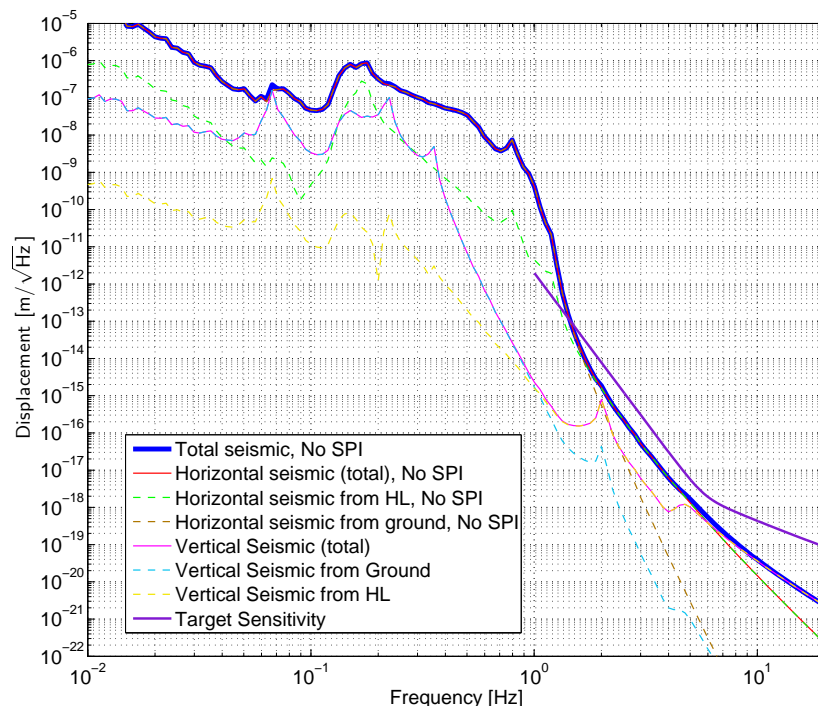


Figure 8: Breakdown of the seismic noise without SPI

Using the stiffness of the heat-links shown in the previous section, the seismic noise introduced through the heat-links are calculated using the suspension model explained in section 2.1. The breakdowns of the seismic noise are shown in figure 8 (without SPI) and figure 9 (with SPI). We used the ground motion spectrum of a normal seismic period and assumed that the motion of the cryo-shield is the same level as the ground motion.

In the case of no SPI, the seismic noise is dominated by the horizontal vibration from the heat-links above 2 Hz. Then it is superseded by the horizontal vibration from the heat-links above 6 Hz. When the SPI is used, the vertical heat-link vibration becomes dominant above 1.5 Hz. In both cases, the vibration introduced from the heat-links does not contaminate the target sensitivity.

3.3 Cryogenic active vibration isolation

The seismic noise in the observation band (above 10 Hz) is dominated by the vertical heat-link vibration. In order to give more safety margin to the seismic noise, we have to suppress the

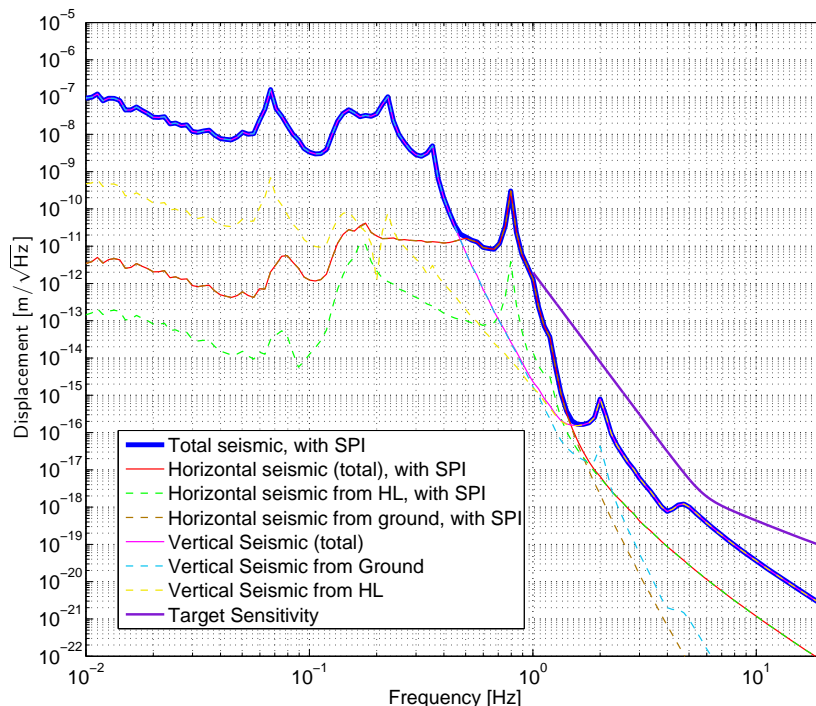


Figure 9: Breakdown of the seismic noise with SPI

vertical heat-link vibration. Since SPI does not work for vertical vibrations, we have to use a scheme which also works for vertical motion.

It is usually a good idea to do an active vibration isolation close to the origin of the vibration source because the vibration is still large and easy to sense. Therefore it is an interesting option to insert an active vibration isolation stage in the heat-link chain just after the 4k shield.

The basic concept of this scheme is shown in figure 10. An accelerometer is connected to the 4k shield through a semi-rigid heat conducting structure such as bellows. This structure should have a good heat conductance so that the temperature of the accelerometer body is almost the same as the 4k shield. At the same time, this connection has to be flexible enough that the accelerometer can be moved relative to the 4k shield to cancel the vibration introduced from the shield. The accelerometer is supported from the ground through an actuator, such as a piezo hexapod, so that the accelerometer can be moved. The vibration sensed by the accelerometer is fed back to the actuator to cancel it. Thus the body of the accelerometer is quieter than the 4k shield. Then the heat-link wires connected to the mirror suspension system is originated from this isolated accelerometer body.

Since loose heat-links may have cross-couplings of vibrations in all DOFs to the in-line direction, active vibration isolation probably has to be performed for all 6 DOFs. Similar vibration isolation systems are demonstrated at the room temperature. The biggest concern for us is whether good cryogenic accelerometers and actuators are available. Piezos are known to work at cryogenic temperatures [1]. There are commercial cryogenic accelerometers using PZTs, but the sensitivity may not be enough for our purpose. We have to investigate on this further more.

3.4 Conclusion for heat-link vibration isolation

The model calculation shows that the vibration introduced from the heat-links does not contaminate the target sensitivity of LCGT. In the observation band, the seismic noise is dominated by the vertical vibration of the heat-links. SPI is not effective to reduce this noise. If we need

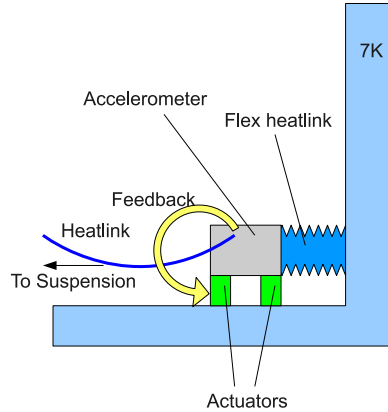


Figure 10: Cryogenic active vibration isolation

further reduction of the seismic noise in the observation band, a new technique such as the cryogenic active vibration isolation is required. The heat-links do not contribute to the RMS motion of the mirrors at all. Therefore, SPI is not necessary from the point of view of the heat-link vibration isolation.

4 Lock acquisition

By the reduction of the RMS mirror motions, an SPI can help the lock acquisition of an interferometer. In this section, we will evaluate the significance of SPI for LCGT lock acquisition. For this purpose, we first summarize the general lock acquisition strategy for LCGT. Then several problems of locking a high finesse cavity are reviewed. Finally we explain two techniques (offset lock and green laser pre-lock) to circumvent these problems.

4.1 LCGT lock acquisition procedure

Lock acquisition is defined as a process to bring the mirrors of an interferometer to the desired operational positions. In the case of a DRFPMI, we have to lock four cavities (two recycling and two arm cavities) and a Michelson interferometer. There are specific steps to be taken to robustly lock all the degrees of freedom.

The first step for the lock acquisition is to lock the central part, i.e. PRC, MICH and SRC. Basically we wait for those three degrees of freedom to come close enough to the operational points by chance to produce sensible error signals. Then the servos draw the mirrors to the operational points. During this process, the arm cavities should not resonate the carrier and the sidebands. Otherwise the resonance will destroy the error signals for the central part.

The error signals used for the initial lock acquisition of the central part have to have wide linear ranges and robustness against the motions of other degrees of freedom. These signals may not be the same as the ones used during the observational operation of the interferometer because the wide range signals generally have higher noise. It is also desirable that the error signals are insensitive to the power build up of the carrier in the PRC and arm cavities. For this purpose, the third order harmonic demodulation or double demodulation between the sidebands are suitable. However, these signals often have smaller linear range. Therefore, we may have to use single demodulation signals for the initial lock and then switch to those carrier insensitive signals before the arm cavities are fully locked. To do this, we need to use the offset lock technique or the green laser pre-lock (explained later in this section) to temporarily prevent the arms from resonating.

After the central part is locked, the arm cavities are locked. If the arm cavities resonate sidebands before they are locked to the carrier, the error signals of the central part will be

disturbed and we may lose the lock. Therefore, it is very important that we lock the arm cavities at the first attempt.

Because of the radiation pressure problem (section 4.2.3), we will lock the arm cavities with some offset from the resonance using the DC transmission power. This is called offset locking. The offset lock error signal has a wider linear range than the conventional Pound-Drever-Hall (PDH) error signal. Offset lock also allows us to switch the error signals of the central part to carrier-insensitive signals such as the third harmonics demodulation.

Finally, we reduce the offsets of the arm cavities slowly to fully lock the interferometer. The error signals for the arm cavity control have to be switched to RF or DC readouts during this process. The servo filters are dynamically changed to compensate for the optical gain change.

The role of the SPI for the lock acquisition is to reduce the RMS speed of the mirrors so that the actuators can easily stop the mirrors at the operational point. This is especially important for the lock of the arm cavities since the finesse of the arm cavities is high (more than 1000). In the following sections, we will focus on the lock of a single Fabry-Perot cavity to evaluate the difficulty of arm cavity lock.

4.2 Obstacles for arm cavity lock

4.2.1 Impulse limit velocity for mass lock acquisition

In order to stop a mirror at a resonance, kinetic energy of the mirror has to be reduced to zero by the test mass actuators. For a high finesse cavity, we can sense the mirror position in a very narrow region around the resonances. The half-width at half-maximum of a cavity resonance in terms of the cavity length is

$$\Delta L = \frac{\lambda}{2\mathcal{F}}. \quad (4)$$

In order to stop the mirror, the impulse given to the mirror from the actuators has to be larger than the initial kinematic energy of the mirror. Therefore, the following inequalities have to be satisfied.

$$\frac{1}{2}m v^2 < F_{\max} \Delta L \quad (5)$$

$$v < v_{\text{impulse}} = \sqrt{2 a_{\max} \Delta L} \quad (6)$$

Here m , v and F_{\max} are mass, speed of the mirror and the maximum force of the actuator, respectively. $a_{\max} = F_{\max}/m$. From the experience at TAMA, the critical mirror velocity (v_c) for a successful lock acquisition is about a half of the above impulse limit velocity v_{impulse} .

The test mass actuators are designed to have

$$\begin{aligned} a_{\max} &= (2\pi f)^2 [1/\text{s}^2] \times \frac{3 \times 10^{-9}}{f^2} [\text{m/V}] \times 10 [\text{V}] \\ &= 1.2 \times 10^{-6} [\text{m/s}^2], \end{aligned} \quad (7)$$

to avoid contamination of the sensitivity from the actuator driver noise.

Impulse limit velocities and critical velocities are listed for various values of finesse in table 1. For the main laser carrier (1064 nm), the critical velocity is very small (16 nm/sec) and it is comparable to the RMS speed of the test masses during a normal seismic period without SPI and during a high seismic period with SPI. Lock acquisition will be very difficult without the SPI when the micro seismic motion is high.

		Finesse \mathcal{F}	ΔL	v_{impulse}	v_c
Arm cavity for 1064 nm for 532 nm	Green Lock	1250	0.426 nm	32 nm/s	16 nm/s
	Green Lock	100	2.660 nm	80 nm/s	40 nm/s
	Green Lock	10	26.60 nm	253 nm/s	126 nm/s

Table 1: Critical velocity of mass lock acquisition

4.2.2 Ringing velocity

A high finesse cavity has a long storage time of photons. This produces a ringing in the transient response of the cavity when the mirrors pass by a resonance. The amount of the ringing depends on the speed of the mirrors. Typical velocity where the ringing becomes significant can be estimated by dividing the resonance width by the storage time. The resonance width of the cavity is represented as $\lambda/2/\mathcal{F}$. Here λ and \mathcal{F} are wavelength of the laser and finesse of the cavity, respectively. The storage time τ is represented as $2L/c \times \mathcal{F}/\pi$. As a result, typical ringing velocity is represented as follows.

$$v_{\text{ringing}} = \frac{\lambda}{2\mathcal{F}} \times \frac{1}{\tau} = \frac{\pi c \lambda}{4L\mathcal{F}^2}$$

Table 2 shows the ringing velocities for several values of arm finesse.

Finesse	Ringing velocity
1550	35 nm/s
1250	53 nm/s
777	138 nm/s
100	4175 nm/s

Table 2: Ringing velocity for several arm finesse values

4.2.3 Radiation pressure

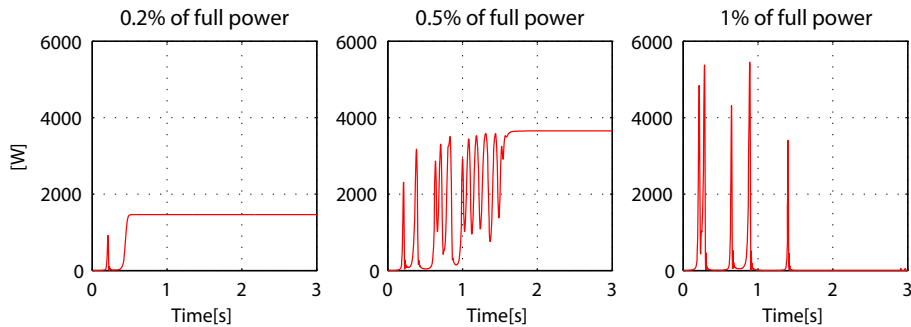


Figure 11: Lock event with the mirror speed of 60 nm/s in various input powers. 0.2% of the full power corresponds to 1.5 kW inside the arm cavity when fully locked. 0.5% and 1% correspond to 3.5 kW and 7 kW respectively.

If the power inside cavity reaches several kW, lock acquisition will be disturbed by the radiation pressure because the pressure kicks the mirrors out of the resonance. This effect was simulated using the E2E simulation engine for a cavity of finesse 1250. In this simulation, a technique called guide lock was used to increase the chance of lock acquisition. In this method, we measure the velocity of the mirror using the first pass of a resonance and then a properly calculated impulse is given to the mirror to gently send it back to the resonant point.

The time series of the cavity power during lock attempts are shown in figure 11 for several input powers. Except for the 0.2% case, the mirrors are kicked by the radiation pressure many times before locked. In the case of 1% power, the cavity could not be locked at all.

The above simulation only took into account the radiation pressure effect in the longitudinal direction. In reality, the radiation pressure also causes an instability in the rotational degrees of freedom. Especially the horizontal push by the radiation pressure induces a pitch tilt of the mirrors. Then the pitch angular instability caused by the radiation pressure is excited and it

could destroy the cavity lock. Figure 12 shows the behavior of the mirror alignment when the arm cavity power is ramped up. The angular radiation pressure induces an oscillation in pitch and eventually the lock is lost.

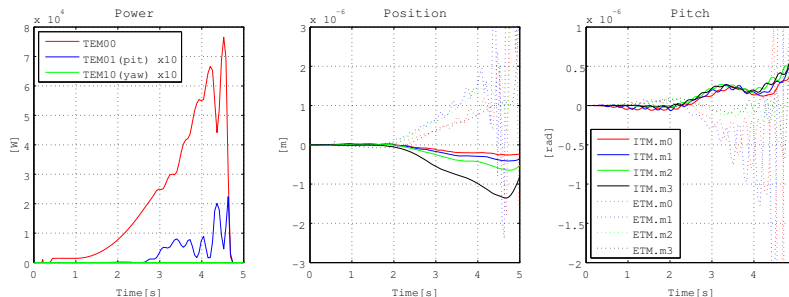


Figure 12: Radiation pressure effects on angle motion without alignment control. Left graph is power inside the cavity. After lock is acquired with very low power, input power is ramped up to full power in 15 seconds. The central graph shows the horizontal position of the mirrors moved by radiation pressure. The right graph shows the pitch angle change. $m0$ to $m3$ refer to the four test masses of an advanced LIGO style quad-suspension. Lock is lost due to the pitch offset when the power inside the cavity reaches about 10 % of full power.

In order to avoid the radiation pressure problems, we have to lock the cavity with a low input power. However, reducing the laser power to 0.2 % of the full power may not be practical as it changes various parameters of the interferometer drastically, especially the power falling onto the detection ports. Offset lock is a way to mitigate this problem and discussed in detail in section 4.3.1.

4.2.4 Arm lock simulation

Here we show simulation results of arm cavity lock using E2E. This simulation was actually done using the parameters of the old advanced LIGO arm cavity design (4 km, finesse 1250) by O. Miyakawa. Since the characteristics of the cavity is very similar to the LCGT arm cavities, we show the results here as a reference. The laser power was largely reduced to eliminate the radiation pressure effect.

In the simulation, the PDH error signal was divided by the transmitted power of the cavity to gain a wider liner region. According to the simulation, it is almost impossible to lock the cavity due to the ringing of the error signal, if the mirror speed exceeds 25 nm/sec.

The probability of successful lock for a single encounter with a resonance was calculated for several different mirror speeds (Table 3). The results indicate that we have to have an extremely slow mirror motion (less than 1 nm/sec) in order to lock the arm cavities at the first attempt using the PDH signals.

Mirror speed	25 nm/s	5 nm/s	2.5 nm/s	0.5 nm/s
Lock probability	9.5%	32%	56%	98%

Table 3: Lock probability with various mirror speeds.

4.3 Advanced lock acquisition techniques

4.3.1 Offset locking

Offset lock is a way to prevent large build up of the carrier power inside an arm cavity. The cavity is first locked at a point far from the resonance using the DC transmitted power as the error signal. This is useful to avoid a strong kick of the mirrors by the radiation pressure. It also gives us a time to switch various error signals and servo topology before building up the

carrier power in the cavities. After the arm cavities are locked with a CARM (common arm length) offset, it is slowly reduced to fully lock the interferometer.

Figure 13 shows results from E2E simulations of offset lock signals. An LCGT arm cavity was swept at various speed and the error signals of offset lock ($1/\sqrt{P_{\text{trans}}}$) are plotted. P_{trans} is normalized to be 1 when the cavity is fully resonant. When the mirrors are moving fast, the cavity cannot build up the power enough. This the reason for the saturation of the error signal around the resonance for high speed cases. In reality, the servo feedback tries to slow down the mirrors. Therefore, the saturation of the error signal will be less significant.

The error signal has a large linear range. We will have to switch between several PDs with different gains to achieve a good error signal over a large range of the transmitted power.

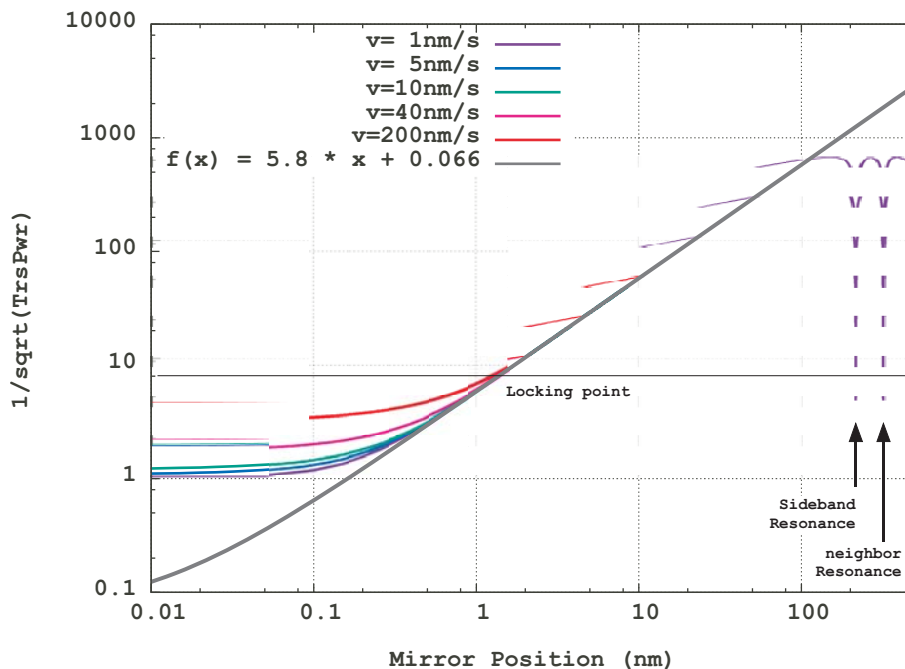


Figure 13: Transmitted light, $1/\sqrt{P_{\text{trans}}} + \text{offset}$ vs Cavity microscopic length. P_{trans} is normalized with the transmission power at the full lock.

4.3.2 Green laser pre-lock

Green laser pre-lock is an advanced technique for lock acquisition proposed by LIGO people [4]. It makes use of frequency doubled Nd:YAG lasers (emit green light) installed at the end stations to lock the arm cavities prior to lock the central part of the interferometer. The arm cavities are kept away from resonances of the carrier and the sidebands of the main laser. In this way, we can avoid disturbances of the error signals from unwanted resonances of the carrier and the sidebands in the arms while attempting to lock the central part.

The green lasers at the end stations are phase locked to the main laser to suppress the relative frequency noise. For this purpose, a small amount of the main laser light is picked off and sent to the end stations through optical fibers. Long fibers may introduce extra phase noises. There is a technique already demonstrated to cancel this noise by sending back a part of the light delivered to the end station through the same fiber [5].

The test mass mirrors are coated with a dichroic coating to have some reflectivities for the green laser. The finesse of the arm cavities is set not too high (~ 100) so that the pre-lock is easy. Actually the laser frequency can be used to initially lock the green laser to the cavities. Therefore, the lock acquisition of the green lasers should be almost instantaneous. After the cavities are locked with the frequency actuators, the feedback points can be handed off to the mirror actuators.

Benefits of green laser pre-lock As was mentioned above, the green pre-lock prevents accidental resonances of the carrier and sidebands in the arms during the initial lock acquisition of the central part. In addition, this scheme allows us to control the microscopic cavity length freely by changing the phase lock frequency. This is a great benefit because then we can always make sure the state of the arm cavities after the central part is locked.

Figure 14 shows a resonance curve of an arm cavity as a function of the cavity length. If we use the offset lock scheme, the cavity length has to be in the non-shaded region after the central part is locked. Otherwise, the cavity has to pass at least one sideband or carrier resonance to reach the desired offset lock point. Also the direction of the mirror motion has to be as indicated by the light blue arrow in the figure. For the offset lock to be successful, both the arm cavities must satisfy these conditions by chance at the time the central part is locked.

If we use the green laser pre-lock, the location of the cavity in the resonance curve can always be pre-determined before the central part is locked. An easiest way to ensure this is to mis-align the PRM and scan the arm cavity length with the green laser lock before attempting to lock the central part.

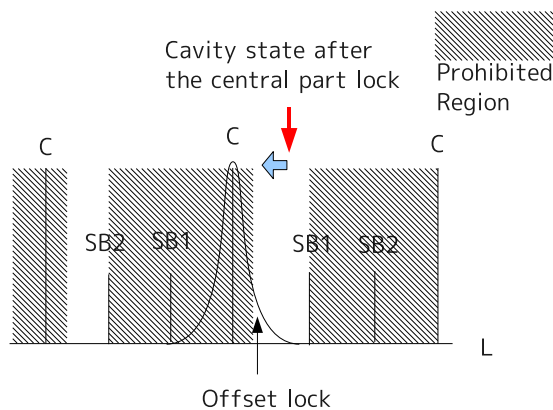


Figure 14: Cavity length conditions for successful offset lock

4.4 Conclusion for lock acquisition

In order to avoid a large kick by radiation pressure, offset lock is inevitable. Offset lock also provides a pause before going to the full lock for switching the error signals and preparing the servo topologies for the full lock.

Since the linear range of the offset lock error signal is very large, we should be able to lock the arm cavities even with the 200 nm/sec RMS speed.

If we implement the green laser pre-lock, the RMS speed of the free swinging mirrors becomes totally irrelevant. Since the green laser pre-lock provides fascinating capabilities for lock acquisition, we should pursue this technique further more.

From these considerations, we conclude that SPI is not essential for lock acquisition.

5 Vacuum tubes

The default diameter of the vacuum tubes for LCGT (1 m) was chosen to accommodate SPI. The scattered light noise was estimated for this tube diameter with two laser beams and confirmed to be a factor of 20 smaller than the requirement[7].

If we do not employ the SPI, but still use the same tube diameter, the safety margin will be much larger. Therefore, there is a room for reducing the beam tube diameter to cut the construction cost. According to our calculations, we can reduce the diameter to 60 cm at the expense of an increase in the estimated scattered light noise by a factor of 1.6 (from $5 \times 10^{-22} \text{m}/\sqrt{\text{Hz}}$ to $8 \times 10^{-22} \text{m}/\sqrt{\text{Hz}}$). Even with this diameter, We still have a safety factor of

75 for the scattered light noise from the design sensitivity. Therefore, we can afford this down scaling if necessary. The estimated cost reduction by this is about 2.5 billion JPY.

However, since the vacuum tubes are hard to replace once they are installed, we have to be careful when choosing smaller diameter tubes. Having large diameter vacuum tubes will allow us to retrofit SPI in the future upgrades or to use larger laser beams when larger mirrors become available.

A Design of the LCGT Suspension Point Interferometer

In this section, we review and discuss the design of the LCGT SPI in order to assess the technical feasibility of the SPI. Although we do not recommend to install an SPI to LCGT as the conclusion of the working group, the current design of the LCGT SPI is presented here for the purpose of documentation of the discussions within the working group.

The first section reviews the working principle of SPI. Then we will present the current design of the LCGT SPI.

A.1 Working Principle

Suspension point interferometer (SPI) is an active vibration isolation scheme for interferometric gravitational wave detectors. The SPI makes use of an auxiliary interferometer to monitor the seismic vibration transmitted through the suspension wires. The seismic vibration is actively suppressed by an appropriate feedback control using the signal from the auxiliary interferometer. The name “suspension point interferometer” is used because the auxiliary interferometer is usually placed at the suspension points of the mirrors of the main interferometer.

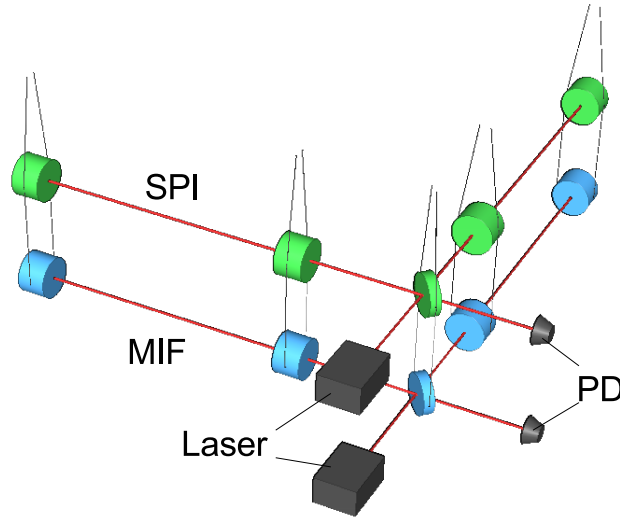


Figure 15: A conceptual configuration of suspension-point interferometers installed to a Fabry-Perot Michelson interferometer

Figure 15 shows a basic configuration of a Fabry-Perot-Michelson interferometer equipped with a suspension point interferometer. The lower interferometer, which is composed of blue optical components in the figure, is called “main interferometer (MIF)” and used to detect gravitational waves. The upper interferometer (colored green in the figure) is called “suspension point interferometer (SPI)”. The vibration transmitted through the wires is monitored by the SPI. Then forces to nullify the vibration are applied to the mirrors of the SPI. Through this, the mirrors of the MIF are isolated from external vibrations.

In this scheme the reference of motion is not the local inertial frame; instead, the SPI measures the same degree of freedom as the MIF, i.e. the distance between the front and end mirrors. Each mirror serves as a reference for its companion mirror. Unlike conventional active vibration isolation schemes using accelerometers, the SPI has a DC performance because the sensor is essentially a position sensor.

In figure 15, the SPI is illustrated as a recombined Fabry-Perot-Michelson interferometer. Actual configuration of the LCGT SPI does not necessarily have to be recombined. The interferometer configuration of the LCGT SPI is discussed in section A.2.1.

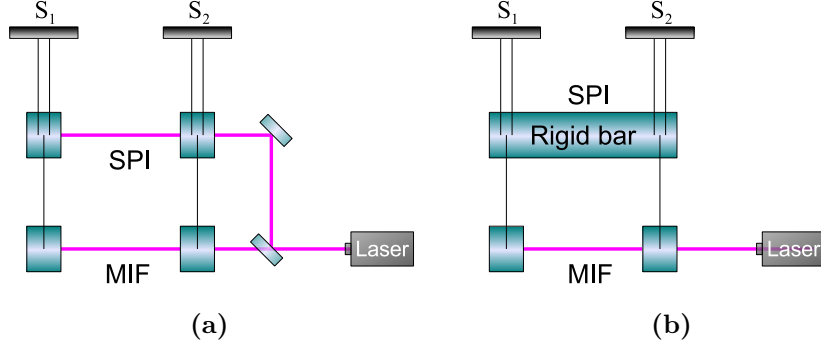


Figure 16: Rigid bar picture of SPI.

A.1.1 Rigid Bar Picture

The working principle of SPI is shown by conceptual drawings in Fig.16. In this case, only a Fabry-Perot arm is shown. Once the SPI is locked, the differential motion of the mirrors of the SPI is suppressed to the accuracy of the servo loop. Therefore, the SPI can be considered as a rigid bar hung across the two suspension systems (Fig.16 (b)). If the pendulums hanging from this virtual rigid bar are identical, no differential motion will be transmitted to the MIF. Consequently the seismic noise in the MIF is significantly reduced. However in reality, the pendulums are not exactly identical. A fraction of the common motion at the SPI stage is converted to differential motion at the MIF by asymmetry of the suspensions.

As a measure of this effect, we define the common mode rejection ratio (CMRR) of SPI as:

$$\text{CMRR} \equiv 2 \left| \frac{H_1(\omega) - H_2(\omega)}{H_1(\omega) + H_2(\omega)} \right| \quad (8)$$

Here $H_1(\omega)$ and $H_2(\omega)$ are the transfer functions of the suspensions hanging below the SPI stage. In the case of single pendulums as shown in Fig.16 (b), the CMRR is approximately written as,

$$\text{CMRR} \simeq |H_1(\omega)| \sqrt{\left(\frac{\Delta l}{g}\right)^2 \omega^4 + \left(\frac{l\gamma}{mg}\right)^2 \left(\frac{\Delta l}{l} + \frac{\Delta\gamma}{\gamma} - \frac{\Delta m}{m}\right)^2 \omega^2}. \quad (9)$$

$$H_1(\omega) \equiv \frac{1}{1 + i\frac{l\gamma}{mg}\omega - \frac{l}{g}\omega^2}, \quad (10)$$

where l , m , γ are the length, mass and damping factor of the pendulum 1 and the letters with Δ represent the difference between the corresponding parameters of the two pendulums. The frequency dependence of CMRR is plotted in Fig.17 in the case of 1% asymmetry. At frequencies higher than the resonance of the pendulum, the CMRR approaches to a plateau at $1/(\omega_1 - \omega_2)^2$, where ω_1 and ω_2 are the resonant frequencies of the pendulums. At lower frequencies the CMRR improves dramatically as the frequency goes down. The CMRR is poor at the resonant frequency. In the case of multiple pendulums, the shape of the CMRR around the resonances changes but the general trend is the same.

CMRR is one of the limiting factors of the performance of an SPI. Other limiting factors includes coupling from other degrees of freedom, servo gain of the SPI, noise of the SPI and so on.

A.2 Design of the LCGT SPI

In this section, we discuss the design of the LCGT SPI.

A.2.1 Interferometer Configuration

There are several possibilities for the interferometer configuration of the LCGT SPI. The most basic one is to use an independent Fabry-Perot cavity for each arm. Since the arm cavities are

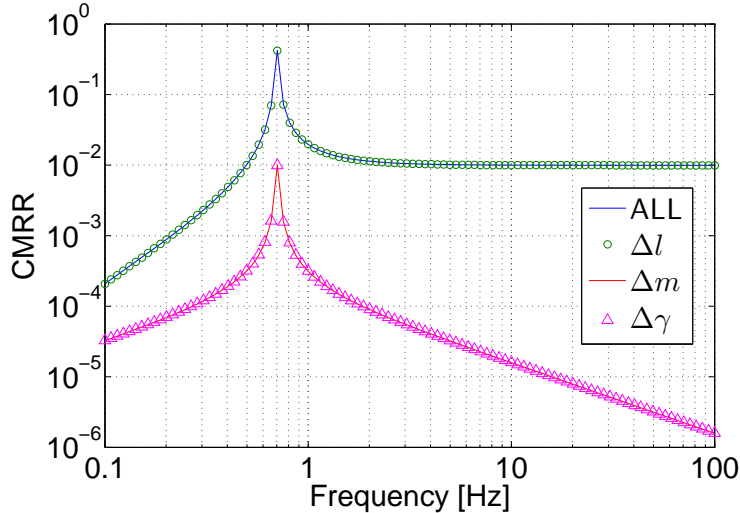


Figure 17: Frequency dependence of CMRR: The blue line shows the CMRR with all asymmetries included. The green circles show the CMRR with only Δl . The red line is the CMRR with only Δm . The pink triangles show the CMRR with only $\Delta \gamma$. All asymmetries are 1%.

most important both in terms of the noise reduction and lock acquisition, this configuration is the baseline design for the LCGT SPI.

By using more complex interferometer configurations similar to the main interferometer, we can suppress the motions in the auxiliary degrees of freedom, such as MICH, PRCL and SRCL. In general, the coupling of the motions in those DOFs to the GW channel is much smaller than the arm cavity contribution. Moreover, the suspensions used for the auxiliary mirrors (PRM, BS, SRM) are not inferior to the ones used for the main optics. Therefore, the vibration noises of the aux. DOFs are expected to be the same order as the arm cavities. This means it is not necessary to further suppress the vibrations in the aux. DOFs by SPI.

Heat links are not attached to the PRM, BS and SRM, thus no need to worry about the extra noise introduced. However, the ITMs will be connected to the largest number of heat links among the core optics in order to subtract large heat generated by the laser light passing through the substrate. As mentioned in section A.1.1, the common motion of the two mirrors forming an arm cavity is not suppressed by the baseline SPI. This common motion is seen as the MICH motion by the main interferometer. In general, the contribution of MICH to the GW channel is smaller than the arm cavities roughly by a factor of finesse. The finesse of the LCGT arm cavity is at least 500. Therefore, if the MICH seismic noise from the heat-links is more than 500 times larger than the target displacement noise of the interferometer, we need an SPI for MICH, i.e. the SPI has to be a recombined Fabry-Perot Michelson interferometer. However, as we see in section 3, this is unlikely to be the case.

The other benefit of introducing the SPI for auxiliary DOFs is to alleviate the coupling of the shot noises in the auxiliary DOFs through the feedback loops. The story goes like this: Usually, the shot noises of the error signals for the auxiliary DOFs are not as good as the one for the GW signal because they do not use the full carrier power enhanced by the arm cavities. Since we feed back those noisier signals to control the auxiliary DOFs, these DOFs move more than the main DOF (the differential arm length). These noises are coupled to the GW channel through non-diagonal elements in the sensing matrix. This is called the loop noise. It can be reduced if we can reduce the feedback bandwidth of the auxiliary DOFs. By using the SPI for those DOFs, we can reduce the RMS motion of the aux. DOFs, which enables us to use smaller control bandwidths. However, according to the simulation study in the interferometer bandwidth working group, the loop noise coupling can be made small enough by choosing appropriate signal ports and a moderate feed forward gain without compromising the feedback bandwidth of the auxiliary DOFs [9].

The basic operation of the baseline SPI (a simple Fabry-Perot) was demonstrated [8]. However, stabilization of the auxiliary DOFs using SPI has not yet demonstrated experimentally.

A.2.2 Location of SPI in the Suspension Chain

In the previous sections, the SPI is assumed to be formed at the penultimate stages of the suspensions. This is the default choice of location for the LCGT SPI. However, there are several other choices for the location of the SPI in the suspension chain.

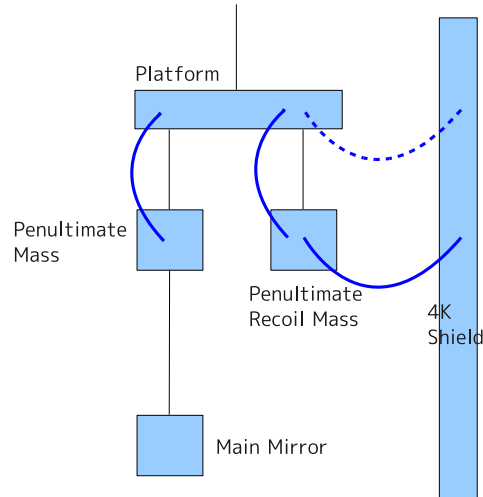


Figure 18: A conceptual diagram of the LCGT cryogenic suspension.

Figure 18 shows a conceptual diagram of the cryogenic suspension of LCGT. Heat-link wires are shown in blue curves. There are two possibilities for the first anchor point of the heat-links, the suspension platform and the penultimate recoil mass.

If we anchor the heat-links on the recoil mass for the penultimate stage, we could form an SPI using these masses to suppress the heat-link vibrations. One advantage of this configuration is that we can prevent or greatly relieve the independent alignment problem, which is discussed in section A.2.3. Another advantage is that we can sense the heat-link vibration before it gets attenuated, therefore, the noise requirement for the SPI will be less stringent.

However, we cannot use the actuator acting between the recoil mass and the penultimate mass. If we do so, the feedback force to cancel the heat-link vibration will also actuate the penultimate mass. This will just copy the heat-link vibration onto the penultimate mass, thus making the situation worse. Therefore, we have to prepare another set of actuators to control the SPI on the recoil masses.

Another problem with this configuration is the inter-degree-of-freedom couplings caused by the heat-link. An SPI formed by the penultimate recoil masses will only suppress the heat-link vibration in the in-line DOF. Therefore, the penultimate recoil mass will still be largely shaken in, for example, the perpendicular direction to the beam by the heat-links. Since the heat-links are soft and loose wires, it is possible that this perpendicular motion is converted to the in-line motion at the next stage. The amount of this kind of coupling has to be experimentally evaluated.

One last disadvantage of the penultimate recoil mass SPI is that it cannot suppress the seismic vibration coming from the above. We could still copy the quietness of the recoil mass to the penultimate mass by using a local sensor between the two masses. However, the applicable frequency will still be severely limited by the noise of the local sensor.

If we do not anchor the heat-link on the penultimate recoil mass (like shown by the dashed heat-link in figure 18 and this is the default configuration), we could use the suspension platforms as SPI masses. This configuration can suppress both the seismic and heat-link vibrations. Al-

though the orientations of the platform and the main mirror are still coupled, we may be able to decouple them by counter actuating the penultimate mass (see the discussions in section A.2.3).

The biggest problem of the platform SPI is that the platform is not exposed to the beam tube in the default design. In order to directly expose it to the tube, we have to make the tube very large. Steering the beam down to the vacuum tube height by hanging a periscope like structure is possible but it will complicate the system unnecessarily.

A.2.3 Suspension Design

There is no detailed design for the suspension of the LCGT SPI mirrors yet. In this section, we describe a conceptual design and discuss the problems to be solved. In this section, the location of the SPI mirror is assumed to be the penultimate stage of the suspension chain.

One big problem of SPI for the practical implementation is that the orientations of the SPI mirror and the main mirror hung from it are strongly coupled. Since the laser beams for the SPI and the main interferometer are not perfectly parallel, we need to adjust the alignment of the SPI and MIF mirrors independently. If we simply rotate the whole SPI stage, the main mirror necessarily follow this rotation. Counter rotating the main mirror by actuators on the main mirror is not a good idea because the actuators on the mirror are designed to be weak enough not to introduce actuator noise.

If the angular actuation range of the main mass actuator is θ_{max} , the actuator noise spectrum can be naively calculated by the following formula [6],

$$x_n(f) = r \frac{m}{I_m} \frac{V_{max}}{V_n} \left(\frac{f}{f_0} \right)^2 \theta_{max} \quad (11)$$

where r is the distance between the actuators (we assumed that four actuators are attached on the back of the mirror), m and I_m are the mass and the moment of inertia of the main mirror, V_{max} and V_n are the maximum input voltage and the input equivalent noise of the actuator driver and f_0 is the resonant frequency of the main mirror in the rotational degree of freedom in question. The estimated actuator noise is plotted using $r = 0.1$ m, $m = 30$ kg, $I_m = 0.176$ kg \cdot m², $V_{max} = 10$ V, $V_n = 1$ nV/ $\sqrt{\text{Hz}}$, $f_0 = 0.8$ Hz and $\theta_{max} = 5 \times 10^{-6}$ rad, along with the classical noise budget of LCGT (figure A.2.3).

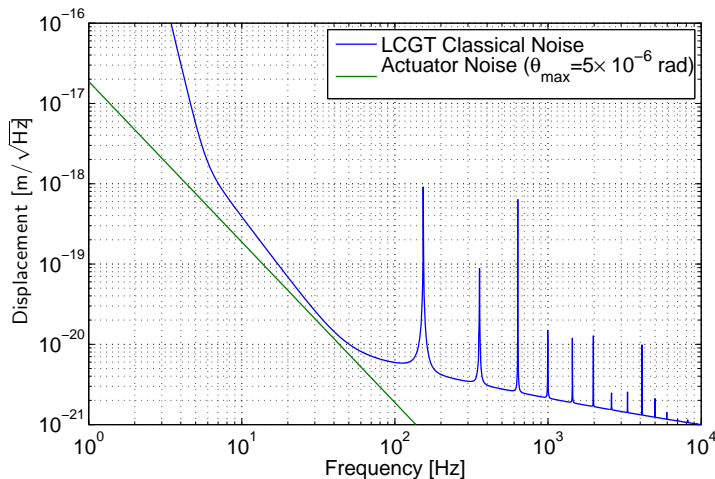


Figure 19: Actuator noise of the main mirror and the classical noise of LCGT

This result means that we can have only have 5×10^{-6} rad $\approx 3 \times 10^{-4}$ deg. of angular actuation range. This is obviously not enough. As suggested in [6], we could allocate dedicated actuators for rotational degrees of freedom, which has only a small coupling (like 1/100) to the in-line direction. However, even a 1/100 coupling would allow us to move the mirror only by

3×10^{-2} deg. Moreover, we do not want to attach many actuators on the main mirror because they may increase the thermal noise.

Since the counter actuation does not seem promising, we have to do some trick to the SPI mirror. The basic idea is to make the SPI mirror a composite structure and rotate the reflective surface with respect to the body. A conceptual design is shown in figure 20.

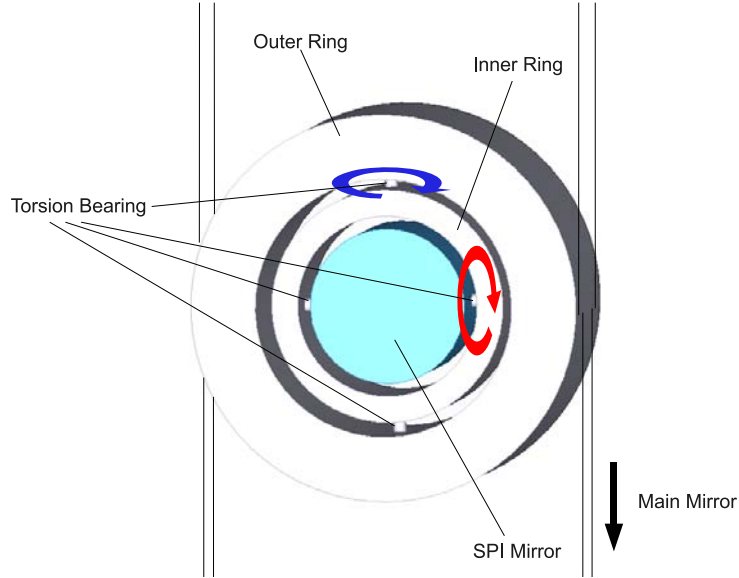


Figure 20: A conceptual design of the SPI mirror suspension

The SPI mirror is supported from the outer ring (the body of the SPI stage) by a gimbal structure through torsion bearings. Therefore, the mirror can be rotated with respect to the outer ring. We will attach coil magnet actuators on the mirror and apply internal (rotational) forces between the outer ring and the mirror to adjust the orientation of the mirror. The main mirror is hung from the outer ring, therefore it is not moved by the adjustment to the SPI mirror orientation.

Since this configuration supports the mirror through a complicated rigid structure, the mechanical quality factor will be degraded. Although the thermal noise requirement for the SPI mirror is not as stringent as the one for the main mirror, still we have to carefully check this before employing this idea.

The other worry is that the torsion bearings may have some mechanical resonances in the observation band. This may contaminate the sensitivity of the main interferometer. Also the mechanical resonances may limit the UGF of the SPI servo hence limiting the SPI's ability to suppress vibrations.

There exists only a conceptual idea for the SPI suspension at this moment. We need more R&D on this in order to implement an SPI for LCGT in practice.

A.2.4 Noise Requirement

The noise requirement of the LCGT SPI, if its optical configuration is an independent Fabry-Perot cavity for each arm, is plotted in Fig. 21 as a gray curve. The noise of the SPI is fed back to the SPI mirror by the servo. This vibration is transmitted to the test mass through the final pendulum of the suspension system. The noise requirement is calculated by requiring that the noise introduced from the SPI is less than the estimated classical noises for the main interferometer by a safety factor of 10. Since the quantum noise becomes dominant for the main interferometer at frequencies above 10 Hz or so, this requirement is more stringent than necessary. But we adopted this approach as the quantum noise level of the LCGT's target sensitivity is still not fully decided.

Assuming that the loop gain of SPI servo has a simple f^{-1} shape and its bandwidth is 50 Hz, the contributions of various noises are calculated.

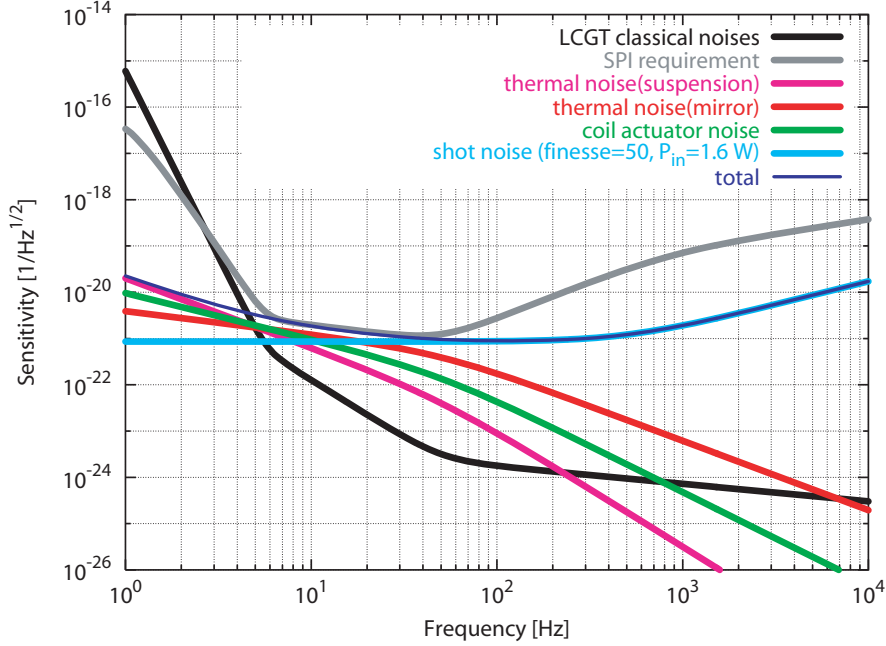


Figure 21: Noise requirement of the LCGT SPI. This requirement is calculated from the LCGT classical noises, a transfer function of the final stage suspension ($f_c = 0.8$ Hz, $Q = 1000$) and a safety factor of 10.

Thermal noise of suspension: At frequencies higher than the resonant frequency of the suspension, the suspension thermal noise has a $f^{-2.5}$ dependence. Since the suspension thermal noise is a real vibration of the SPI mass, the SPI suppresses this noise. Therefore the requirement for the suspension thermal noise above the SPI stage is relieved by the SPI's servo gain. Quantitatively, the requirement of the suspension thermal noise can be written as:

$$h_{\text{thermal(suspension)}} < 1 \times 10^{-18} \times f^{-2.5} \text{ 1}/\sqrt{\text{Hz}}, \quad (12)$$

$$x_{\text{thermal(suspension)}} < 3 \times 10^{-15} \times f^{-2.5} \text{ m}/\sqrt{\text{Hz}}. \quad (13)$$

Thermal noise of mirror: The thermal noise of mirror has a $f^{-0.5}$ dependence and increases the noise level of the MIF because it is converted to length motion by the SPI servo. Therefore, the requirement of the mirror thermal noise is written as:

$$h_{\text{thermal(mirror)}} < 3.9 \times 10^{-21} \times f^{-0.5} \text{ 1}/\sqrt{\text{Hz}}, \quad (14)$$

$$x_{\text{thermal(mirror)}} < 1.2 \times 10^{-17} \times f^{-0.5} \text{ m}/\sqrt{\text{Hz}}. \quad (15)$$

In order to realize this requirement, Q-factor of the mirror should be higher than 165 if the mirror geometry is a simple cylindrical shape. However, since actual mirror geometry of the SPI mass is complicated as shown in Fig. 20, we will need to analyze it more in detail.

Coil driver noise: Coil driver noise has a f^{-2} dependence at a higher frequency than the resonant frequency of the suspension. It is suppressed by the SPI servo within the control bandwidth. The requirement for the raw coil driver noise (without the servo suppression) is:

$$h_{\text{coil}} < 4.8 \times 10^{-19} \times f^{-2} \text{ 1}/\sqrt{\text{Hz}}, \quad (16)$$

$$x_{\text{coil}} < 1.4 \times 10^{-15} \times f^{-2} \text{ m}/\sqrt{\text{Hz}}. \quad (17)$$

If the coil driver noise is $1 \text{ nV}/\sqrt{\text{Hz}}$, we have to choose the actuator efficiency to be less than $1.4 \times 10^{-6}/f^2 \text{ m/V}$. Assuming that we use operational amplifiers with the output voltage range of $\pm 15\text{V}$ and the suspension's resonant frequency is 0.8 Hz , the maximum actuation range is $66 \mu\text{m}$.

Shot noise: Since the noise requirement in the high frequency is decreased by the final stage suspension, the shot noise level can be chosen relatively freely as shown in Fig. 22. The lower the finesse of the cavities is, the easier the lock acquisition is. However, since acceptable laser power on PD is limited, finesse of 50 seems to be a better solution.

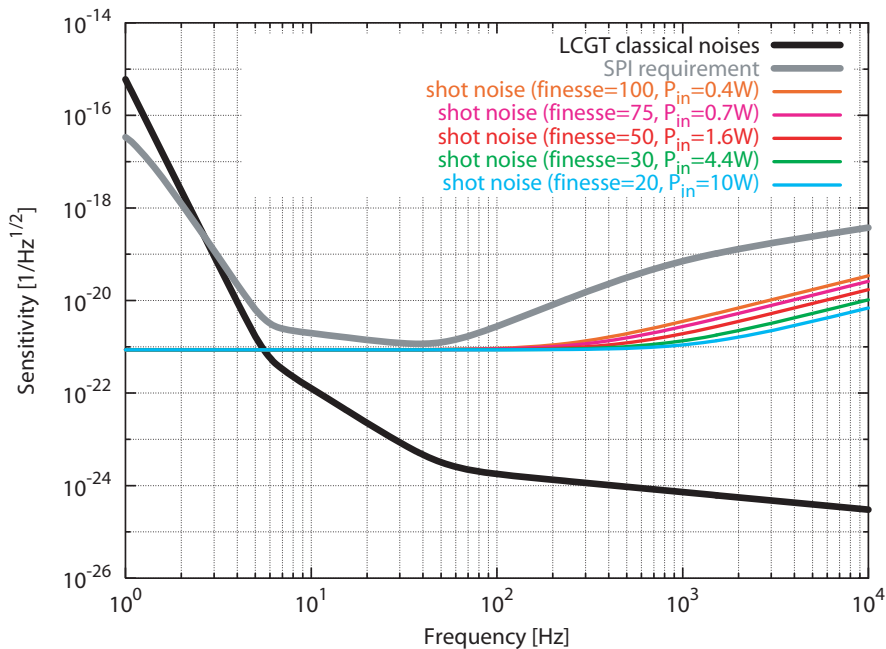


Figure 22: Shot noise. Laser power and finesse of the arm cavities can be chosen relatively freely.

A.2.5 Input Optics

A laser for the SPI should be phase-locked to the main laser. We can select two solutions to obtain a phase-locked laser beam. One is to pick up a fraction of the main laser as shown in Fig. 23, and the other is that another laser is prepared and is phase-locked to the main laser as shown in Fig. 24. Since each configuration has some advantages and disadvantages, we describe them in the following.

First, we describe the configuration shown in Fig. 23. The biggest advantage of this configuration is that it does not require any control system for phase locking. In addition, laser power available is not limited severely. A disadvantage of this configuration is that the SPI operation is affected by the MIF's operation directly.

The configuration shown in Fig. 24 uses a fiber coupled secondary laser for SPI. The biggest advantage of this configuration is that we can lead laser beam to MMT4 easily by using an optical fiber. However, we must suppress the noises induced by the optical fiber. Another advantage is that SPI operation is relatively independent of the MIF. Even if the MIF loses lock, the SPI may be able to stay locked. This configuration has two disadvantages. One is that we need a tight phase-lock control of the secondary laser. The other one is that the available laser power is limited to about 2 W which is the highest power of commercial laser with reliable performance to be used in a gravitational wave detector.

Since the length of Fabry-Perot cavities in SPI is stabilized relative to the frequency of the laser, the phase-locked loop for the secondary needs a large enough gain to stabilize the laser

frequency of a free running laser to that of the SPI requirement shown in Fig. 21. Typically, a frequency noise of an NPRO is $300 \text{ Hz}/\sqrt{\text{Hz}}$ at 100 Hz, which is equivalent to a strain sensitivity of $1 \times 10^{-12} / \sqrt{\text{Hz}}$ at 100 Hz. Accordingly, the loop gain needed for the phase lock is about 10^9 at 100 Hz. In addition, a photo detector with low noise and high current capacity is needed for the phase lock.

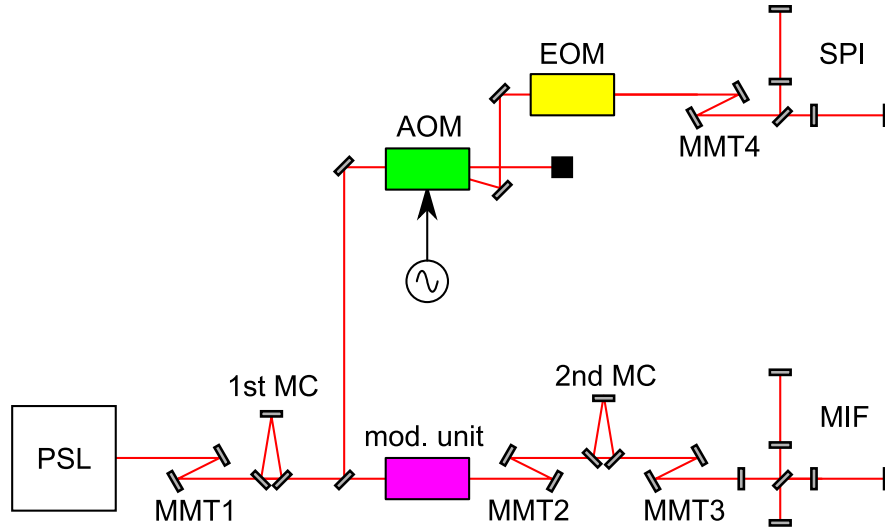


Figure 23: Optical configuration (A). The laser light for the SPI is picked off from the main laser.

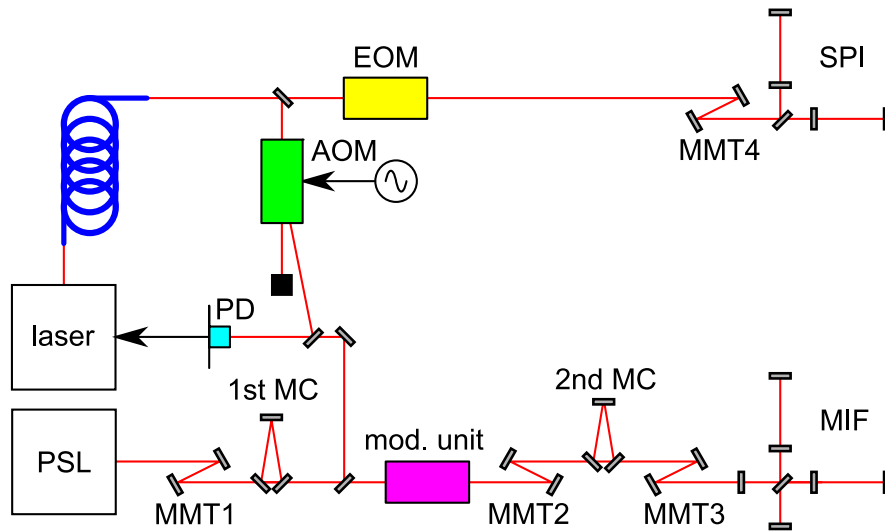


Figure 24: Optical configuration (B). A dedicated laser, which is phase-locked to the main laser, is used for the SPI.

A.2.6 Comments on technical feasibility

The biggest problem for the practical implementation of the SPI for LCGT is the independent alignment of the test masses and the SPI mirrors. The proposed suspension design to mitigate this problem is only a conceptual one and requires a detailed analysis and experimental tests.

Since the structure of the SPI masses is expected to be complex, we may have to deal with extra mechanical resonances, which might compromise the sensitivity of the main interferometer.

There is no demonstration of SPI with interferometer configurations other than a Fabry-Perot. If we need to install the SPI to auxiliary DOFs, this is a big uncertainty. We will need to do a prototype experiment for this.

B Members of the working group

Chair: Yoichi Aso (University of Tokyo)
Masaki Ando (Kyoto University), Koji Arai (Caltech), Kiwamu Izumi (NAOJ)
Osamu Miyakawa (ICRR), Shinji Miyoki (ICRR), Shigenori Moriwaki (University of Tokyo)
Shigeo Nagano (NICT), Noriaki Ohmae (University of Tokyo), Kentaro Somiya (Caltech)
Toshikazu Suzuki (KEK), Ryutaro Takahashi (NAOJ), Daisuke Tatsumi (NAOJ)
Takashi Uchiyama (ICRR) and the LCGT SPI special working group.

C Acronyms

- PRC: Power Recycling Cavity
- PRCL: Power Recycling Cavity Length
- SRC: Signal Recycling Cavity
- SRCL: Signal Recycling Cavity Length
- MICH: Michelson
- CARM: Common arm length
- DARM: Differential arm length
- MIF: Main Interferometer
- PDH: Pound Drever Hall
- DOF: Degree(s) Of Freedom
- ROC: Radius Of Curvature

References

- [1] R. Vaccarone, A. Pozzo and R. Puppò, *Physica B* **284** (2000) 2115
- [2] Virgo Collaboration, *Astroparticle Physics*, **20** (2004) 629
- [3] O. Miyakawa *et al*, *Phys. Rev. D* **74**, 022001 (2006)
- [4] P. Fritschel *et al*, Adv. LIGO Arm Length Stabilisation Design, LIGO Document T0900144 (2009)
- [5] P. A. Williams, W. C. Swann, and N. R. Newbury, *J. Opt. Soc. Am. B*, **25**(8), 1284 (2008)
- [6] , LCGT Design Document version 2 (2007)
- [7] R. Takahashi and Y. Saito, *Vacuum*, in press, available from <http://dx.doi.org/10.1016/j.vacuum.2009.06.059>
- [8] Y. Aso, PhD thesis, University of Tokyo 2006, available from http://granite.phys.s.u-tokyo.ac.jp/theses/aso_d.pdf
- [9] LCGT interferometer bandwidth special working group report, 2009